Acta Crystallographica Section D
Biological Crystallography
ISSN 0907-4449

The structure of an MDM2–Nutlin-3a complex solved by the use of a validated MDM2 surface-entropy reduction mutant

Burcu Anil,[a] Christiane Riedinger,[a] Jane A. Endicott[b] and Martin E. M. Noble[b]*

[a]Department of Biochemistry, University of Oxford, South Parks Road, Oxford OX1 3QU, England, and [b]Northern Institute for Cancer Research, Newcastle University, Framlington Place, Newcastle Upon Tyne NE2 4HH, England

Correspondence e-mail: martin.noble@ncl.ac.uk

Received 31 October 2012
Accepted 14 February 2013

PDB References: MDM2–p53 peptide complex, 4hfz; MDM2–Nutlin-3a complex, 4hg7

The p53-binding site of MDM2 holds great promise as a target for therapeutic intervention in MDM2-amplified p53 wild-type forms of cancer. Despite the extensive validation of this strategy, there are relatively few crystallographically determined co-complex structures for small-molecular inhibitors of the MDM2–p53 interaction available in the PDB. Here, a surface-entropy reduction mutant of the N-terminal domain of MDM2 that has been designed to enhance crystallogenesis is presented. This mutant has been validated by comparative ligand-binding studies using differential scanning fluorimetry and fluorescence polarization anisotropy and by cocrystallization with a peptide derived from p53. Using this mutant, the cocrystal structure of MDM2 with the benchmark inhibitor Nutlin-3a has been determined, revealing subtle differences from the previously described co-complex of MDM2 with Nutlin-2.

1. Introduction

The transcription factor p53 is the major tumour suppressor of the cell and plays a central role in the regulation of many cellular mechanisms such as apoptosis, DNA repair, angiogenesis, survival and senescence (Lane, 1992; Vogelstein *et al.*, 2000; Fridman & Lowe, 2003). The *p53* gene is altered in 50% of cancers and the function of p53 is down-regulated in cancers where the wild-type protein is retained (Hainaut & Hollstein, 2000; Brown *et al.*, 2009). Murine double minute 2 (MDM2) is the major cellular antagonist of p53 and is over-expressed or amplified in various cancers (Watanabe *et al.*, 1992; Momand *et al.*, 1998). MDM2 and p53 are autoregulated through a negative-feedback loop in which p53 binds to the *MDM2* gene promoter upon activation and induces MDM2 expression. The increase in the level of MDM2 causes the protein to inhibit the function of p53, which is carried out through three different mechanisms (Picksley & Lane, 1993). The N-terminal domain of MDM2 binds to the transactivation domain of p53 and hence blocks its activity as a transcription factor (Oliner *et al.*, 1992). MDM2 also contains a nuclear export signal that is used to shuttle p53 into the cytoplasm (Tao & Levine, 1999). Finally, MDM2, which has E3 ligase activity, targets p53 for proteasomal degradation by ubiquitylation (Haupt *et al.*, 1997; Honda *et al.*, 1997; Wade *et al.*, 2010).

The MDM2–p53 interaction is mainly mediated by the N-terminal domains of both proteins (Chen *et al.*, 1993; Picksley *et al.*, 1994). The crystal structure of MDM2 in complex with p53 (residues 15–29) shows that the interaction is largely mediated by three key residues of p53, namely Phe19, Trp23 and Leu26, and the binding surface on MDM2 is well defined (Kussie *et al.*, 1996). The structural nature and

the critical role of the MDM2–p53 interaction in regulating p53 levels have led to the exploration of this interaction as a therapeutic target. Various classes of small nonpeptidic inhibitors that target MDM2 have been reported (Riedinger & McDonnell, 2009; Weber, 2010). MDM2 inhibitors that have been widely studied include the Nutlins (Vassilev *et al.*, 2004), the spiro-oxindoles (Ding *et al.*, 2005), the benzodiazepinediones (Grasberger *et al.*, 2005) and the isoindolinones (Hardcastle *et al.*, 2005, 2006, 2011; Riedinger *et al.*, 2008; Watson *et al.*, 2011). Further series of small-molecule inhibitors with high potency towards MDM2 have been reported, including indolyl hydantoins (Graves *et al.*, 2012), piperidinones (Rew *et al.*, 2012) and imidazolyl indoles (Furet *et al.*, 2012).

Despite intense interest in MDM2 as a target for anticancer drug discovery, only ten small-molecule cocrystal structures have been deposited in the PDB (Vassilev *et al.*, 2004; Ding *et al.*, 2005; Grasberger *et al.*, 2005; Allen *et al.*, 2009; Popowicz *et al.*, 2010; Furet *et al.*, 2012; Graves *et al.*, 2012; Rew *et al.*, 2012). This relative paucity of structural data reflects the challenges presented in crystallizing the p53-binding domain of MDM2, which is relatively flexible in its apo form (Uhrinova *et al.*, 2005; Showalter *et al.*, 2008) and which may have a surface composition that is not conducive to crystallization: MDM2–ligand complex crystal structures show that lattice stabilization is often achieved through interactions of the ligands rather than interactions of the MDM2 domain alone (see, for example, Vassilev *et al.*, 2004; Furet *et al.*, 2012). The ability of the ligands to increase the stability of MDM2 and to provide crystal contacts makes the presence of a high-affinity ligand a prerequisite for crystallization of MDM2. Therefore, new crystallization conditions need to be determined for each ligand–MDM2 complex.

The mutation of proteins and protein complexes so that they will consistently yield diffraction-quality crystals is an approach that has been in increasingly wide use (Dale *et al.*, 2003; Bonnefond *et al.*, 2011). One method, which was first suggested by Derewenda, is the engineering of protein surfaces (Derewenda, 2004). In this strategy, termed 'surface-entropy reduction' (SER), the entropic penalty that is introduced into the crystallization process by the large polar side chains of amino acids such as lysine, glutamate and glutamine is reduced by the mutation of these residues to alanine. Lysine, glutamate and glutamine, particularly where they occur in clusters, are the most suitable targets for mutagenesis since they occur on the protein surface with a high incidence (Baud & Karlin, 1999) and are rarely involved in protein–protein interactions (Lo Conte *et al.*, 1999). Their mutation to alanine is also thought to expose backbone carbonyl and amide groups that form networks of hydrogen bonds with the surrounding water molecules; these networks are disrupted upon the formation of crystal contacts, thereby providing a further entropic advantage to the crystallization process (Derewenda, 2011).

In order to obtain consistent crystallization conditions that would yield diffraction-quality crystals, we have applied the SER approach to the N-terminal domain of MDM2 and validated one of the resulting mutants for use in the support of structure-based drug discovery. Here, we describe the crystal structure of MDM2 in complex with the benchmark compound Nutlin-3a generated using this method.

2. Materials and methods

2.1. Protein expression and purification

The fragment $MDM2_{17–108}$ was amplified from a pGEX6P1 plasmid (GE Life Sciences) into which $MDM2_{17–125}$ had been cloned using the restriction enzymes *Bam*HI and *Xho*I. The amplified fragment was cloned into the same vector using the same sites. Point mutations were introduced into the $MDM2_{17–108}$ template stepwise through whole-plasmid PCR amplification using complementary primers introducing the nucleotide changes. The plasmids were transformed into *Escherichia coli* strain BL21 (DE3). The proteins were produced as GST fusions in 5 l flasks using 1 l of either lysogeny broth (LB) medium (wild type) or Hyper-Broth (Molecular Dimensions; mutants) supplemented with 100 µg ml^{-1} carbenicillin. Cultures were grown to an OD_{600} of 0.6 at 310 K and induced at 291 K by the addition of IPTG to a final concentration of 0.2 m*M*. Protein expression was maintained overnight. Constructs were purified on glutathione beads (GE Life Sciences) followed by cleavage of the GST tag by PreScission 3C protease. The cleaved proteins were loaded onto a Superdex S200 HR 26/60 column with a running buffer consisting of 20 m*M* HEPES, 100 m*M* NaCl, 5 m*M* dithiothreitol (DTT), 0.02% NaN_3 at pH 7.4.

2.2. Thermal denaturation screening assay

The intrinsic thermal stability (T_m) and the change in T_m caused by ligand binding (ΔT_m) were evaluated using differential scanning fluorimetry (Pantoliano *et al.*, 2001). Following optimization of the assay to return the best fluorescent signal, concentrations of 5 µ*M* (wild-type protein) or 9 µ*M* (mutated proteins) were used in a solution that also contained 20 m*M* HEPES pH 7.4, 100 m*M* NaCl, 5 m*M* DTT, 0.02% NaN_3. SYPRO Orange (Sigma) was used as the fluorescent probe at a concentration of 10 µ*M*. The experiments were carried out in 96-well low-profile Thermo-Fast plates on a Stratagene RT PCR 305. Ligands were added to the sample wells at a 1:2 molar ratio, with DMSO present as a co-solvent at a final concentration in the range 0–2.5% as required. The final sample volume was 20 µl in each well. After mixing, the plates were sealed and spun down at 850*g* for 1 min. Fluorescent signal readings were taken between 298 and 362 K in 0.5 K increments with an equilibration time of 1 min at each point. All experiments were repeated three times.

2.3. Fluorescence polarization measurements

The binding of a p53-derived peptide corresponding to residues 15–29 ($p53_{15–29}$; sequence SQETFSDLWKLLPEN) labelled with fluorescein at its N-terminus was measured using fluorescence polarization (FP) assays. Measurements were made using a PHERAstar^{Plus} plate reader (BMG Labtech) in

384-well Corning black microtitre plates with an excitation wavelength of 485 nm and an emission wavelength of 530 nm. The binding constant of the peptide was determined for $MDM2_{17–108}$ and MDM2_E69AK70A *via* saturation binding experiments. In different experiments, fluorescently labelled peptide was used at concentrations of 5, 10 or 15 n*M*. Protein was added to a final concentration in the range 0.04–51.2 µ*M*. Inhibitor K_i values were determined through competition assays in which the protein, at a concentration corresponding to 90% of the measured K_d (*i.e.* 400 n*M* for $MDM2_{17–108}$ and 1700 n*M* for MDM2_E69AK70A), was pre-incubated with 15 n*M* fluorescently labelled peptide. The fluorescence anisotropy in the presence of varying concentrations of competitor (in the range 2–32 768 n*M*) was then measured. Data were analysed using the Cheng–Prusoff equation (Cheng & Prusoff, 1973). The data were fitted using *SigmaPlot* (v.12) intrinsic ligand-binding equations.

2.4. Protein preparation for crystallography

$p53_{15–29}$ was obtained from Severn Biotech Ltd (Worcestershire, England) at a purity of 95.1%. The protein–peptide complex was prepared by incubating the peptide at a concentration of 300 µ*M* with 150 µ*M* MDM2_E69AK70A at 277 K overnight. The complex was purified on a Superdex S75 column in a running buffer consisting of 20 m*M* HEPES pH 7.4, 100 m*M* NaCl, 5 m*M* DTT, 0.02% NaN_3. The complex was concentrated to 11 mg ml^{-1} using a Vivaspin sample concentrator with a molecular-weight cutoff of 5000 Da. Crystals of the complex were grown by the sitting-drop method at 277 K from 0.2 *M* ammonium sulfate pH 4.6, 30%(*w*/*v*) PEG 8000. Needle-shaped crystals belonging to space group $P4_32_12$, with unit-cell parameters $a = b = 52.9$, $c = 196.2$ Å, grew in 1–2 weeks. Subsequent analysis showed that the crystals contained two molecules in the asymmetric unit. The crystals were cryoprotected in 30% ethylene glycol, 70% reservoir solution and were flash-cooled in liquid nitrogen. Data were collected using a PILATUS 6M detector (DECTRIS) on beamline ID29 at the European Synchrotron Radiation Facility (ESRF).

Nutlin-3a was obtained as a powder from Cayman Chemicals and was dissolved in DMSO to prepare a stock at 40 m*M*. The compound was added to a 100 µ*M* stock of MDM2_E69AK70A to give a final concentration of 200 µ*M*. The mixture was incubated at 277 K overnight. The sample was concentrated to 10 mg ml^{-1} using a Vivaspin sample concentrator with a molecular-weight cutoff of 3000 Da, washed twice with the abovementioned HEPES buffer and concentrated to 15 mg ml^{-1}. Crystals were grown by the sitting-drop method at 277 K from 0.5 *M* ammonium sulfate, 0.1 *M* sodium citrate pH 5.6, 1.0 *M* lithium sulfate (a condition from Structure Screen I + II, Molecular Dimensions). Oval-shaped crystals belonging to space group $P6_522$, with unit-cell parameters $a = b = 71.5$, $c = 104.2$ Å, grew in approximately five weeks. The crystals were cryoprotected in 30% ethylene glycol, 70% reservoir solution and were flash-cooled in liquid nitrogen. Data were collected using a Mar225 CCD detector (MAR Research) on beamline ID23-2 at the ESRF.

Table 1
Data-collection and refinement statistics.

	MDM2_E69AK70A–p53	MDM2_E69AK70A–Nutlin-3a
Data collection		
Wavelength (Å)	0.96	0.8726
Space group	$P4_32_12$	$P6_522$
Unit-cell parameters (Å, °)	$a = b = 52.9$, $c = 196.2$, $\alpha = \beta = \gamma = 90$	$a = b = 71.4$, $c = 104.2$, $\alpha = \beta = 90$, $\gamma = 120$
Resolution (Å)	46.7–2.7 (2.85–2.69)	33.8–1.6 (1.69–1.60)
Total reflections	39954	74251
Unique reflections	8223	21274
Completeness (%)	98.9 (99.8)	99.5 (99.5)
R_{merge}† (%)	9.6 (43.0)	6.7 (50.5)
$\langle I/\sigma(I)\rangle$	14.3 (4.9)	11.9 (2.7)
Refinement		
Resolution (Å)	51.1–2.69 (2.76–2.69)	30.9–1.60 (1.64–1.60)
R_{work}‡ (%)	19.5 (23.8)	17.3 (23.6)
R_{free}§ (%)	24.7 (38.5)	21.4 (30.6)
No. of atoms		
Protein	1431	790
Peptide/ligand	190	40
Solvent/ion	70	111
Average *B* factor (Å^2)	24.8	21.6
Root-mean-square deviation from ideality		
Bond lengths (Å)	0.01	0.01
Bond angles (°)	1.6	1.6
Main-chain torsions¶ (%)	100	100

† $R_{merge} = \sum_{hkl}\sum_i |I_i(hkl) - \langle I(hkl)\rangle| / \sum_{hkl}\sum_i I_i(hkl)$, where $I_i(hkl)$ is the *i*th observation of a reflection with Miller indices *hkl*. ‡ $R_{work} = \sum_{hkl} ||F_{obs}| - |F_{calc}|| / \sum_{hkl} |F_{obs}|$, where F_{obs} and F_{calc} are the observed and calculated structure factor and the summation is over reflections included in the refinement. § R_{free} is an equivalent summation to R_{work} for a 5% set of reflections excluded from refinement. ¶ Main-chain torsions gives the percentage of amino acids in the structures that are indicated by *Coot* to have φ and ψ torsion angles that fall within the allowed regions of the Ramachandran plot.

2.5. Crystallographic data processing, model building and refinement

All data were indexed and integrated using the *XDS* package (Kabsch, 2010) and were further processed using the *CCP*4 suite (Winn *et al.*, 2011). The MDM2_E69AK70A–p53 peptide structure was solved by molecular replacement using the published MDM2–p53 complex structure (PDB entry 1ycr; Kussie *et al.*, 1996) as a search model in *Phaser* (McCoy *et al.*, 2007). The MDM2_E69AK70A–Nutlin-3a complex structure was solved in the same way using a modified version of the 1ycr structure in which the peptide coordinates were omitted. Refinement was carried out using *REFMAC*5 (Murshudov *et al.*, 2011) and *BUSTER* (Bricogne *et al.*, 2011), and manual rebuilding was performed with *Coot* (Emsley & Cowtan, 2004). Representative electron density for the two structures is presented in Supplementary Fig. S1.[1] Data-collection and refinement statistics are given in Table 1.

3. Results and discussion

3.1. Choice of constructs

The N-terminal domain of MDM2 has three clusters of lysines and glutamates on the surface of the protein (Lys51-Glu52, Glu69-Lys70 and Lys94-Glu95) that are suitable for

[1] Supplementary material has been deposited in the IUCr electronic archive (Reference: MN5020). Services for accessing this material are described at the back of the journal.

SER. These residues are remote from the p53-binding site and are therefore not expected to interfere with ligand binding. Constructs spanning the residue range 17–125 of MDM2 have most frequently been used in previous structural studies (see, for example, Kussie *et al.*, 1996). However, residues 109–125 form a largely unstructured tail, and the high entropy of this tail, which may become restricted in the crystal lattice, might disfavour the crystallization process. We therefore generated constructs in which the protein was truncated at residue 108 and in which the surface residues listed above were mutated to alanine singly and in pairs. We proceeded to validate and attempt crystallization trials with an $MDM2_{17–108}$ construct in which Glu69 and Lys70 were mutated to alanine, since this construct (termed MDM2_E69AK70A) produced the greatest amount of protein when expressed recombinantly. While we identified these amino acids by visual inspection, we note that the *SERp* server (Goldschmidt *et al.*, 2007) identifies these two amino acids as suitable targets for SER mutation.

3.2. Construct validation by differential scanning fluorimetry

To validate the MDM2_E69AK70A mutant for use in structure-based drug design, we first set out to establish whether the mutations perturb the ligand-binding properties

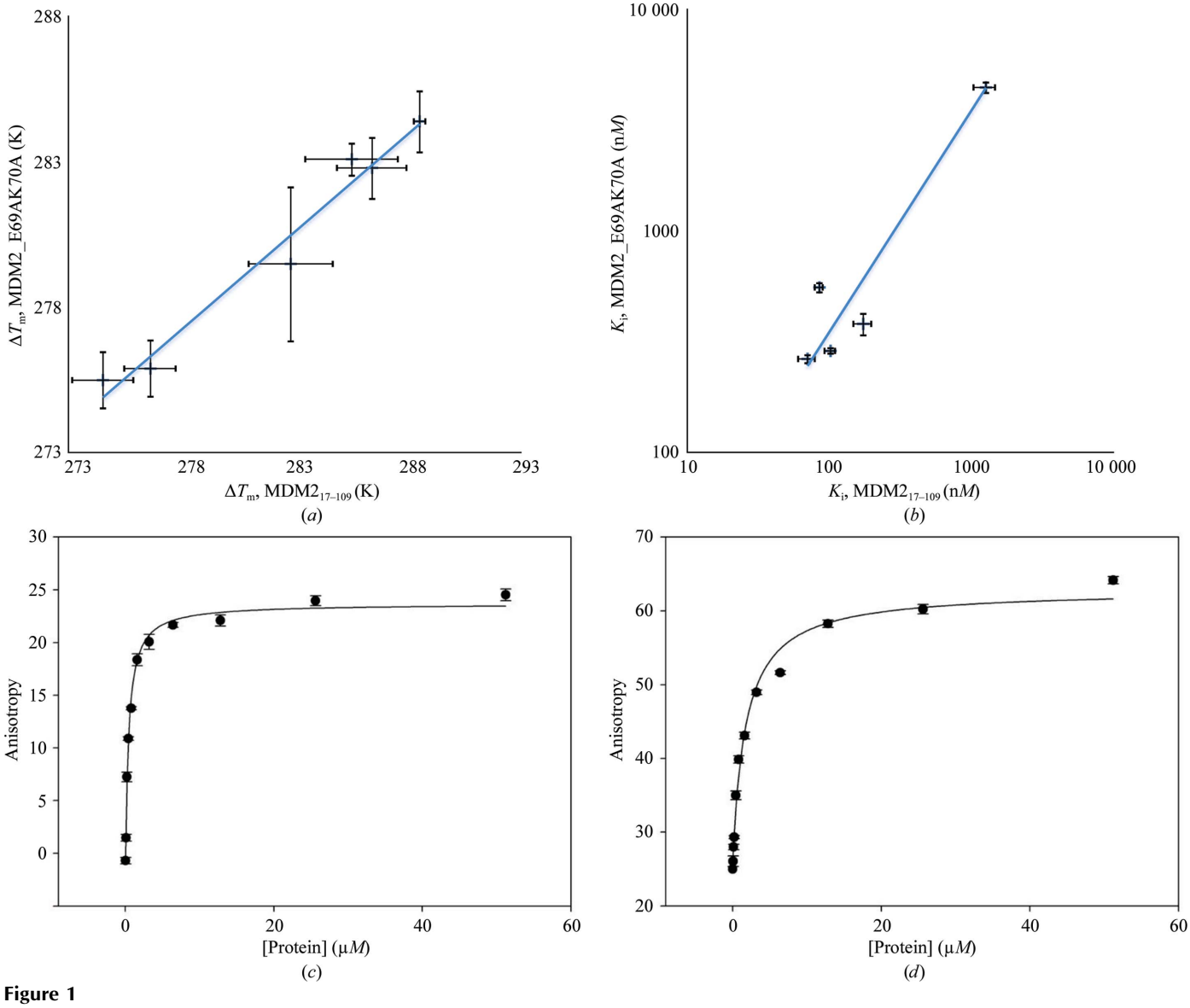

Figure 1
Ligand binding to $MDM2_{17–108}$ and MDM2_E69AK70A characterized by differential scanning fluorimetry (DSF) and fluorescence polarization anisotropy (FP). (*a*) Correlation of ΔT_m for $MDM2_{17–108}$ and MDM2_E69AK70A. The ΔT_m values for the two domains are the change in melting temperature that results from the addition of DMSO, $p53_{15–29}$, Nutlin-3a, MI-63, compound 1 or compound 2 (see Supplementary Figs. S2 and S3 for the raw DSF data and for the structural formulae of the compounds used here, respectively, and Supplementary Table S1 for the derived T_m values). (*b*) Correlation of the K_i values of $MDM2_{17–108}$ and MDM2_E69AK70A, where the K_i values are the inhibition constants for interference with the binding of fluorescein-labelled $p53_{15–29}$ to either $MDM2_{17–108}$ (*x* axis) or MDM2_E69AK70A (*y* axis) evaluated by fluorescence polarization anisotropy. Data are presented for the competitive ligands $p53_{15–29}$, Nutlin-3a, MI-63, compound 1 and compound 2 (see Supplementary Figs. S4 and S3 for the raw FP data and the structural formulae of the compounds used here, respectively, and Supplementary Table S2 for the derived K_i values). (*c*, *d*) Raw FP data for the binding of fluorescein-labelled $p53_{15–29}$ to either $MDM2_{17–108}$ (*c*) or MDM2_E69AK70A (*d*).

of the domain. To this end, we measured the melting temperature (T_m) of both wild-type $MDM2_{17–108}$ and the MDM2_E69AK70A mutant in the apo form and in the presence of a range of ligands using differential scanning fluorimetry. Without any ligand bound, the surface mutations decrease the T_m of $MDM2_{17–108}$ by 3.9 K (Supplementary Figs. S2*a* and S2*b* and Table S1). Glutamate-to-alanine mutations have been shown elsewhere to decrease the stability of proteins without necessarily compromising crystallogenesis (Mateja *et al.*, 2002).

The T_m values of $MDM2_{17–108}$ and MDM2_E69AK70A were then determined in the presence of a range of ligands including a p53-derived peptide ($p53_{15–29}$), Nutlin-3a, MI-63 and two isoindolinone inhibitors (compound 1 and compound 2; Supplementary Figure S3). There is a simple linear relationship between the measured values of the ligand-induced change in T_m (ΔT_m) for the two constructs (Fig. 1*a*), with a linear correlation coefficient (R^2) of 0.97. The ΔT_m values for MDM2_E69AK70A bound to the ligands are lower by an average of 2.2 K than those of the wild-type protein, presumably because the destabilization induced by the mutations introduces a small and constant entropic penalty to the order-promoting process of ligand binding. The strong linear correlation confirms that the mutations do not compromise the validity of structural or biophysical experiments conducted with MDM2_E69AK70A.

3.3. Construct validation by fluorescence polarization

To further explore the ligand-binding properties of the wild-type and mutant proteins, we determined the binding affinity of $p53_{15–29}$ to $MDM2_{17–108}$ and MDM2_E69AK70A by fluorescence polarization (FP). The K_d for fluorescein-labelled $p53_{15–29}$ was around five times lower for the wild-type protein (K_d = 401 ± 34 n*M*; Fig. 1*c*) than for MDM2_E69AK70A (K_d = 1900 ± 200 n*M*; Fig. 1*d*), which is consistent with the decreased ligand affinity of the mutated domain described above. We subsequently expanded the FP study to investigate the release of fluorescent $p53_{15–29}$ from MDM2 in competitive binding studies with each of the ligands listed above (Supplementary Table S2 and Fig. S4). Again, a strong linear relationship is revealed between the K_i values for interaction with $MDM2_{17–108}$ and MDM2_E69AK70A (R^2 = 0.99; Fig. 1*b*), further validating the mutant for use as a surrogate for the wild-type domain in structural and biophysical assays.

3.4. Construct validation by cocrystallization with a p53-derived peptide

To structurally characterize MDM2_E69AK70A, we attempted cocrystallization with $p53_{15–29}$ using commercial screens and custom screens spanning conditions known from previous crystallization studies of MDM2 (Kussie *et al.*, 1996; Vassilev *et al.*, 2004; Grasberger *et al.*, 2005). Crystals grew in a number of different conditions (Supplementary Figs. S5*a*–S5*c*) and we solved the crystal structure at 2.7 Å resolution using one of these crystals.

$p53_{15–29}$ binds to MDM2_E69AK70A and to the wild-type protein (as presented in PDB entry 1ycr) in a similar fashion (Fig. 2). Phe19 and Trp23 fill the pockets on MDM2 identically, although Leu26 in the MDM2_E69AK70A structure is not as deeply buried in the corresponding pocket as it is in the wild-type structure. The residues following the small α-helix of the peptide adopt a more helical conformation in the MDM2_E69AK70A complex than in the complex with the wild-type protein. A comparison of the MDM2_E69AK70A–$p53_{15–29}$ structure with those of MDM2 in complex with diverse peptides available in the PDB confirms that this region most frequently adopts a helical conformation in MDM2–peptide complexes (data not shown). For this reason, the structure that we observe here may be more representative of the authentic interaction than the conformation in 1ycr. Notably, the residues which differ in conformation are involved in lattice contacts in the 1ycr structure (see below).

3.5. Crystallization and structure determination of MDM2_E69AK70A–Nutlin-3a

To determine the structure of an MDM2–Nutlin-3a co-complex, we set up crystallization trials of $MDM2_{17–108}$ and MDM2_E69AK70A constructs in the presence of Nutlin-3a. While the MDM2_E69AK70A trays yielded a large number of crystalline hits (Supplementary Figs. S5*d*–5*f*), all solid phases formed in the drops in the wild-type trays were either amorphous precipitates or hair-like crystallites and did not improve in optimization screens (data not shown). We therefore proceeded with the MDM2_E69AK70A crystals and solved the structure bound to Nutlin-3a at 1.6 Å resolution.

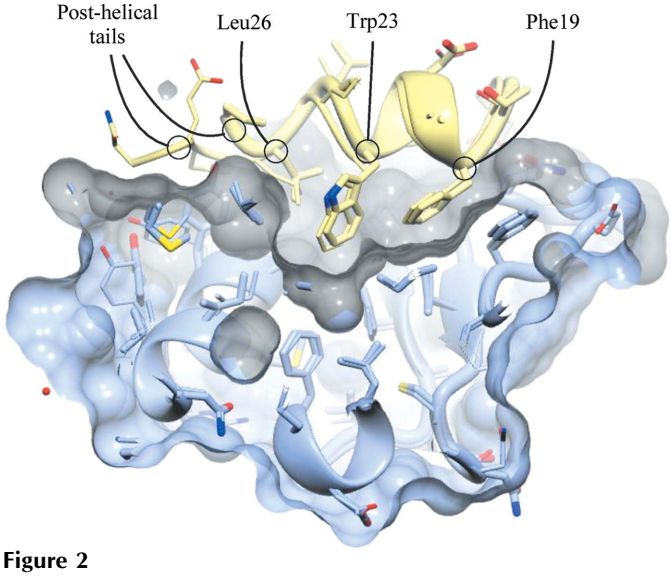

Figure 2
Comparison of the structure of $p53_{15–29}$ bound to MDM2_E69E70A with that of the same peptide bound to $MDM2_{17–125}$ (PDB entry 1ycr). p53 peptides are shown as ribbon and cylinder representations with C atoms coloured yellow. The MDM2 domains are shown as ribbon and cylinder representations with C atoms coloured ice-blue. The MDM2_E69AK70A structure is drawn with thicker representations, while the 1ycr structure is drawn with thinner representations. The molecular surface of MDM2_E69AK70A is coloured ice-blue, except where it defines amino acids within 4 Å or atoms of the ligand, where it is coloured grey.

Nutlin-3a binds to the N-terminal domain of MDM2 with a similar pose to that observed for Nutlin-2 in PDB entry 1rv1 (Vassilev *et al.*, 2004; Fig. 3). For both inhibitors, the halophenyl rings fill the Trp23 and Leu26 pockets. However, the 2-isopropoxy-4-methoxyphenyl group at position 2 in Nutlin-3a is tilted further towards the protein compared with the equivalent 2-ethoxy-4-methoxyphenyl group in Nutlin-2. The piperazin-2-one group points out of the peptide-binding cleft, forming a polar interaction with the peripheral side chain of Gln72, whereas the corresponding methanone group in Nutlin-2 is relatively tilted by an angle of approximately 90°.

The conformation of MDM2 is very similar in the two complexes, although some of the residues in close contact with the inhibitors display differences. For example, the side chain of Tyr100 is tilted by approximately 85° in the structure bound to Nutlin-3a compared with that bound to Nutlin-2 and packs against the side chains of Met52 and Leu54. The loop spanned by residues 67–72 also shows differences between the two structures, such that closer polar contacts are formed between Gln72 and the inhibitor in the Nutlin-3a-bound structure. In addition, the Leu26 pocket is slightly better filled in the Nutlin-3a complex than in the Nutlin-2 complex, with the chlorophenyl ring of Nutlin-3a being more closely packed against the His96 and Tyr100 side chains (Fig. 3*b*). These differences are consistent with the higher potency measured for Nutlin-3a (IC_{50} = 90 n*M*) than for Nutlin-2 (IC_{50} = 140 n*M*) (Vassilev *et al.*, 2004). The loop formed by MDM2 residues 17–25 points outwards in the MDM2_E69AK70A–$p53_{15–29}$ complex. These residues partially pack onto the protein in the Nutlin-3a complex structure, which is consistent with an earlier hypothesis that these residues can provide a hydrophobic cover to either a protein surface patch or to hydrophobic ligands (Showalter *et al.*, 2008).

Leu33 is replaced by a glutamate residue in the Nutlin-2 complex structure (PDB entry 1rv1). This mutation was introduced into the protein in order to increase the surface charge and thus improve the solubility (Vassilev *et al.*, 2004). A glutamate at position 33 is also present in the crystal structure of MDM2 in complex with an indolyl hydantoin (PDB entry 3vbg; Graves *et al.*, 2012) and with an imidazolyl indole (PDB entry 4dij; Furet *et al.*, 2012). In our structure the authentic leucine residue was preserved. Glu33 is involved in intermolecular crystal contacts in the 1rv1 and 3vbg structures but not in the 4dij structure, and the equivalent amino acid in our MDM2_E69AK70A–Nutlin-3a structure, Leu33, is also involved in crystal contacts.

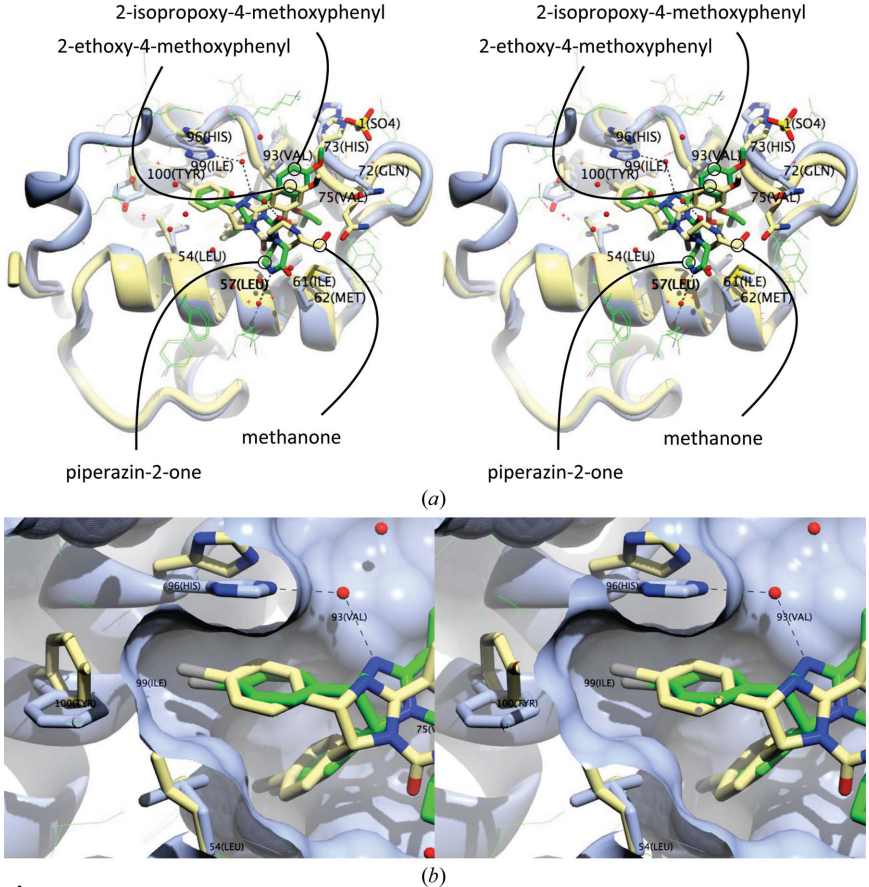

Figure 3
The structure of an MDM2_E69AK70A–Nutlin-3a complex compared with that of an MDM2–Nutlin-2 complex. (*a*) Atomic detail of the complex. The MDM2_E69AK70A structure is shown as an ice-blue ribbon representation with residues that contact Nutlin-3a directly (<4 Å) displayed in cylinder representation and with C atoms coloured blue. The corresponding Nutlin-3a molecule is shown in cylinder representation with C atoms coloured green. The structure of chain *A* of the Nutlin-2 complex (PDB entry 1rv1) is shown as a yellow ribbon representation with residues that contact Nutlin-2 directly (<4 Å) displayed in cylinder representation with C atoms coloured yellow. The corresponding Nutlin-2 molecule is shown in cylinder representation with C atoms coloured yellow. (*b*) The encapsulation of the chlorophenyl groups in the Leu26 pockets of the Nutlin-3a and Nutlin-2 complexes. The same representations as in (*a*) are shown with the addition of the molecular surface of the MDM2_E69AK70A domain (coloured ice-blue). Repositioning of His96 and rotation of the side chain of Tyr100 lead to a closer fit around the group from Nutlin-3a.

3.6. Establishing the mechanism of enhanced crystallogenesis

To explore the contribution of the mutations to crystallogenesis, we first evaluated the involvement of ligands in cocrystal structures of MDM2_E69AK70A using the *PISA* module of *CCP*4*mg*. Crystal contacts are significantly reduced in the MDM2_E69AK70A–$p53_{15–29}$ and the MDM2_E69AK70A–Nutlin-3a complexes compared with the most closely related complexes that lack these mutations (PDB entries 1ycr and 1rv1, respectively; Kussie *et al.*, 1996; Vassilev *et al.*, 2004). In the 1ycr structure the $p53_{15–29}$ peptide shares an interface of 176 Å^2 with a crystallographically related MDM2 molecule and an interface of 64 Å^2 with a crystallographically related p53 peptide, compared with the 722 Å^2 involved in the cognate MDM2–p53 interface (Fig. 4*a*). In our crystals, the only lattice

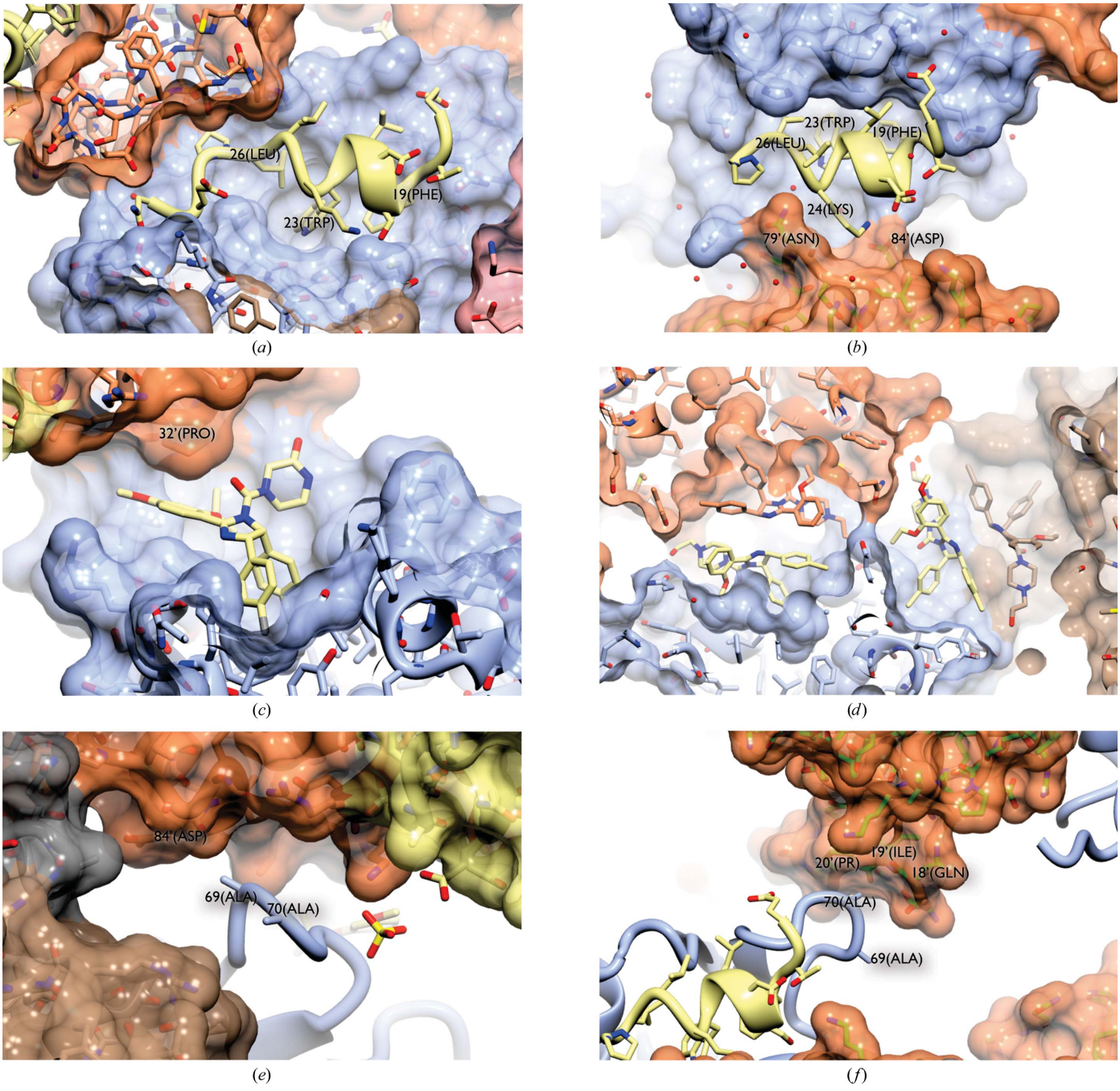

Figure 4
The contribution of the E69A and K70A mutations to crystallogenesis. (*a*) Crystal contacts made by the p53 peptide in the MDM2–p53 complex (PDB entry 1ycr). The peptide is shown in ribbon representation with side chains highlighted in cylinder representation and with C atoms coloured yellow. The cognate MDM2 domain is shown in cylinder representation (with C atoms coloured ice-blue) and in molecular-surface representation (coloured solid ice-blue). Crystallographically related or NCS-related molecules that lie close to the ligand-binding site are shown in cylinder and molecular-surface representations with C atoms (cylinder representation) or all atoms (molecular-surface representation) coloured coral. The only NCS-related or symmetry-related amino acids that contact the central p53 peptide are labelled. (*b*) Corresponding representation of the MDM2–p53 complex in the MDM2_E69AK70A complex. Additional neighbouring molecules are coloured pink, brown and orange. (*c*) Crystal contacts made by Nutlin-3a in the MDM2_E69AK70A–Nutlin-3a complex. The Nutlin-3a molecule is shown in cylinder representation with C atoms coloured yellow. The cognate MDM2 domain is shown in cylinder representation (with C atoms coloured ice-blue) and in molecular-surface representation (coloured solid ice-blue). Crystallographically or NCS-related molecules that lie close to the ligand-binding site are shown in cylinder and molecular-surface representations with C atoms (cylinder representation) or all atoms (molecular-surface representation) coloured coral. (*d*) Corresponding representation of the MDM2–Nutlin-2 complex (PDB entry 1rv1). (*e*) Crystal contacts mediated by the E69AK70A mutations in the MDM2_E69AK70A–p53$_{15–29}$ complex. A molecule of MDM2_E69AK70A is shown in ribbon representation with C atoms coloured ice-blue and with the side chains of Ala69 and Ala70 shown in cylinder representation. Neighbouring molecules within the lattice are shown in molecular-surface and cylinder representation with the molecular surfaces of each chain coloured differently. (*f*) Corresponding representation of the crystal contacts mediated by the E69AK70A mutations in the MDM2_E69AK70A–Nutlin-3a complex. The positions of the mutations in the primary and tertiary structures of MDM2 are highlighted in Supplementary Fig. S5.

interaction made by the peptide has an area of 136 Å^2. This interaction is predominantly contributed by a single side-chain contact between Lys24 of the peptide and Asp84 of a symmetry-related MDM2 molecule (Fig. 4*b*).

In the complex of MDM2 with Nutlin-2 (PDB entry 1rv1; Vassilev *et al.*, 2004), in addition to the cognate Nutlin–MDM2 interface (which has an area in the range 378–389 Å^2 for the three canonically bound Nutlin-2 molecules present in the PDB) inhibitor molecules are also extensively buried in multiple contacts to crystallographically related protein and inhibitor molecules (Fig. 4*d*). The three canonically bound Nutlin-2 molecules present in the PDB form lattice-stabilizing interfaces that total between 273 and 307 Å^2 in size. In contrast, in the MDM2_E69AK70A–Nutlin-3a complex the sole crystallographic contact in which Nutlin-3a participates has an interface area of only 123 Å^2 and the inhibitor primarily contacts the side chain of Pro32 of a crystallographically related complex (Fig. 4*c*).

To further explore the contribution of the mutations to crystallogenesis, we investigated the participation of the mutation sites in lattice stabilization. The double mutation E69A, K70A generates a surface patch that is involved in crystal contacts in both of the novel structures described here. In the complex with $p53_{15–29}$ the alanine residues pack against Gln18, Ile19 and Pro20 of a neighbouring MDM2 molecule (Fig. 4*e*). In the complex with Nutlin-3a the same residues contact residues Gln18, Ile19 and Pro20 of a neighbouring MDM2_E69AK70A molecule in the crystal (Fig. 4*f*).

4. Concluding remarks

In conclusion, we have designed and prepared an SER mutant of MDM2 that fulfills the ambitions of not perturbing comparative ligand binding and enabling crystallographic analysis through generating a novel scope for crystal contacts, consistent with the design hypothesis. The resulting cocrystal structure of MDM2 with Nutlin-3a provides a significant contribution to the growing database of structurally characterized inhibitors of this key protein–protein interaction.

Compound 1 and compound 2 were synthesized by Sarah Cully, Anna Watson and Karen Haggerty, and were kindly provided for our experiments by Dr Ian Hardcastle, Professor Roger Griffin and Professor Bernard Golding, Newcastle University. We thank the staff at the European Synchrotron Radiation Facility beamlines ID23-2 and ID-29 for providing excellent facilities and Edward Lowe for data-collection management.

References

Allen, J. G. *et al.* (2009). *J. Med. Chem.* **52**, 7044–7053.
Baud, F. & Karlin, S. (1999). *Proc. Natl Acad. Sci. USA*, **96**, 12494–12499.
Bonnefond, L., Schellenberger, P., Basquin, J., Demangeat, G., Ritzenthaler, C., Chênevert, R., Balg, C., Frugier, M., Rudinger-Thirion, J., Giegé, R., Lorber, B. & Sauter, C. (2011). *Cryst. Growth Des.* **11**, 4334–4343.
Bricogne, G., Blanc, E., Brandl, M., Flensburg, C., Keller, P., Paciorek, W., Roversi, P., Smart, O. S., Vonrhein, C. & Womack, T. O. (2011). *BUSTER*. Cambridge: Global Phasing Ltd.
Brown, C. J., Lain, S., Verma, C. S., Fersht, A. R. & Lane, D. P. (2009). *Nature Rev. Cancer*, **9**, 862–873.
Chen, J., Marechal, V. & Levine, A. J. (1993). *Mol. Cell Biol.* **13**, 4107–4114.
Cheng, Y. & Prusoff, W. H. (1973). *Biochem. Pharmacol.* **22**, 3099–3108.
Dale, G. E., Oefner, C. & D'Arcy, A. (2003). *J. Struct. Biol.* **142**, 88–97.
Derewenda, Z. S. (2004). *Structure*, **12**, 529–535.
Derewenda, Z. S. (2011). *Acta Cryst.* D**67**, 243–248.
Ding, K., Lu, Y., Nikolovska-Coleska, Z., Qiu, S., Ding, Y., Gao, W., Stuckey, J., Krajewski, K., Roller, P. P., Tomita, Y., Parrish, D. A., Deschamps, J. R. & Wang, S. (2005). *J. Am. Chem. Soc.* **27**, 10130–10131.
Emsley, P. & Cowtan, K. (2004). *Acta Cryst.* D**60**, 2126–2132.
Fridman, J. S. & Lowe, S. W. (2003). *Oncogene*, **22**, 9030–9034.
Furet, P., Chène, P., De Pover, A., Valat, T. S., Lisztwan, J. H., Kallen, J. & Masuya, K. (2012). *Bioorg. Med. Chem. Lett.* **22**, 3498–3502.
Goldschmidt, L., Cooper, D. R., Derewenda, Z. S. & Eisenberg, D. (2007). *Protein Sci.* **16**, 1569–1576.
Grasberger, B. L. *et al.* (2005). *J. Med. Chem.* **48**, 909–912.
Graves, B., Thompson, T., Xia, M., Janson, C., Lukacs, C., Deo, D., Di Lello, P., Fry, D., Garvie, C., Huang, K. S., Gao, L., Tovar, C., Lovey, A., Wanner, J. & Vassilev, L. T. (2012). *Proc. Natl Acad. Sci. USA*, **109**, 11788–11793.
Hainaut, P. & Hollstein, M. (2000). *Adv. Cancer Res.* **77**, 81–137.
Hardcastle, I. R. *et al.* (2005). *Bioorg. Med. Chem. Lett.* **15**, 1515–1520.
Hardcastle, I. R. *et al.* (2006). *J. Med. Chem.* **49**, 6209–6221.
Hardcastle, I. R. *et al.* (2011). *J. Med. Chem.* **54**, 1233–1243.
Haupt, Y., Maya, R., Kazaz, A. & Oren, M. (1997). *Nature (London)*, **387**, 296–299.
Honda, R., Tanaka, H. & Yasuda, H. (1997). *FEBS Lett.* **420**, 25–27.
Kabsch, W. (2010). *Acta Cryst.* D**66**, 125–132.
Kussie, P. H., Gorina, S., Marechal, V., Elenbaas, B., Moreau, J., Levine, A. J. & Pavletich, N. P. (1996). *Science*, **274**, 948–953.
Lane, D. P. (1992). *Nature (London)*, **358**, 15–16.
Lo Conte, L., Chothia, C. & Janin, J. (1999). *J. Mol. Biol.* **285**, 2177–2198.
Mateja, A., Devedjiev, Y., Krowarsch, D., Longenecker, K., Dauter, Z., Otlewski, J. & Derewenda, Z. S. (2002). *Acta Cryst.* D**58**, 1983–1991.
McCoy, A. J., Grosse-Kunstleve, R. W., Adams, P. D., Winn, M. D., Storoni, L. C. & Read, R. J. (2007). *J. Appl. Cryst.* **40**, 658–674.
Momand, J., Jung, D., Wilczynski, S. & Niland, J. (1998). *Nucleic Acids Res.* **26**, 3453–3459.
Murshudov, G. N., Skubák, P., Lebedev, A. A., Pannu, N. S., Steiner, R. A., Nicholls, R. A., Winn, M. D., Long, F. & Vagin, A. A. (2011). *Acta Cryst.* D**67**, 355–367.
Oliner, J. D., Kinzler, K. W., Meltzer, P. S., George, D. L. & Vogelstein, B. (1992). *Nature (London)*, **358**, 80–83.
Pantoliano, M. W., Petrella, E. C., Kwasnoski, J. D., Lobanov, V. S., Myslik, J., Graf, E., Carver, T., Asel, E., Springer, B. A., Lane, P. & Salemme, F. R. (2001). *J. Biomol. Screen.* **6**, 429–440.
Picksley, S. M. & Lane, D. P. (1993). *Bioessays*, **15**, 689–690.
Picksley, S. M., Vojtesek, B., Sparks, A. & Lane, D. P. (1994). *Oncogene*, **9**, 2523–2529.
Popowicz, G. M., Czarna, A., Wolf, S., Wang, K., Wang, W., Dömling, A. & Holak, T. A. (2010). *Cell Cycle*, **15**, 1104–1111.
Rew, Y. *et al.* (2012). *J. Med. Chem.* 55, 4936–4954.
Riedinger, C., Endicott, J. A., Kemp, S. J., Smyth, L. A., Watson, A., Valeur, E., Golding, B. T., Griffin, R. J., Hardcastle, I. R., Noble, M. E. M. & McDonnell, J. M. (2008). *J. Am. Chem. Soc.* **130**, 16038–16044.
Riedinger, C. & McDonnell, J. M. (2009). *Future Med. Chem.* **1**, 1075–1094.

Showalter, S. A., Bruschweiler-Li, L., Johnson, E., Zhang, F. & Brüschweiler, R. (2008). *J. Am. Chem. Soc.* **130**, 6472–6478.
Tao, W. & Levine, A. J. (1999). *Proc. Natl Acad. Sci. USA*, **96**, 3077–3080.
Uhrinova, S., Uhrin, D., Powers, H., Watt, K., Zheleva, D., Fischer, P., McInnes, C. & Barlow, P. N. (2005). *J. Mol. Biol.* **350**, 587–598.
Vassilev, L. T., Vu, B. T., Graves, B., Carvajal, D., Podlaski, F., Filipovic, Z., Kong, N., Kammlott, U., Lukacs, C., Klein, C., Fotouhi, N. & Liu, E. A. (2004). *Science*, **303**, 844–848.
Vogelstein, B., Lane, D. & Levine, A. J. (2000). *Nature (London)*, **408**, 307–310.
Wade, M., Wang, Y. V. & Wahl, G. M. (2010). *Trends Cell Biol.* **20**, 299–309.
Watanabe, T., Ichikawa, A., Saito, H. & Hotta, T. (1992). *Leuk. Lymphoma*, **21**, 391–397.
Watson, A. F. *et al.* (2011). *Bioorg. Med. Chem. Lett.* **21**, 5916–5919.
Weber, L. (2010). *Expert Opin. Ther. Pat.* **20**, 179–191.
Winn, M. D. *et al.* (2011). *Acta Cryst.* D**67**, 235–242.